The Innovation, Volume *5*

Supplemental Information

Stable organic radical qubits and their applications in quantum information science

Aimei Zhou, Zhecheng Sun, and Lei Sun

The Innovation

Supplemental Information

Table of Contents

Triphenylmethyl radicals

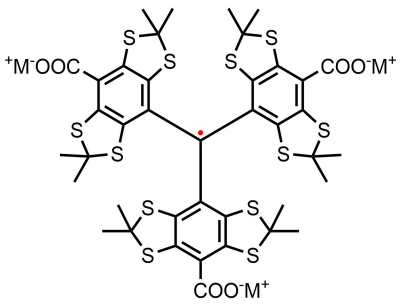

Trityl-CH_3

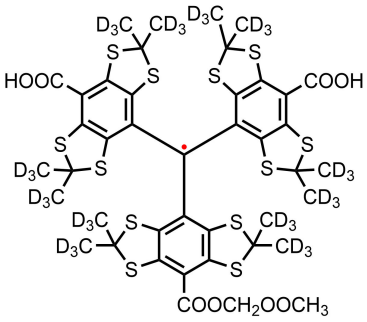

$FDAM_1$

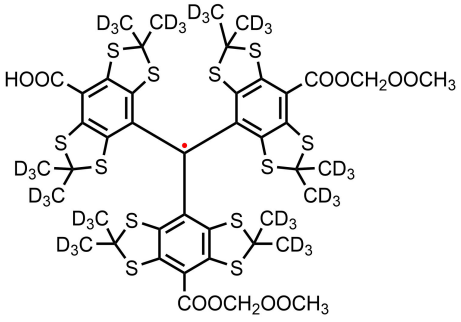

$FDAM_2$

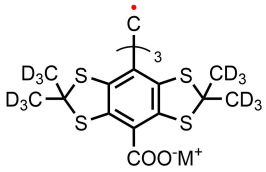

Trityl-CD_3

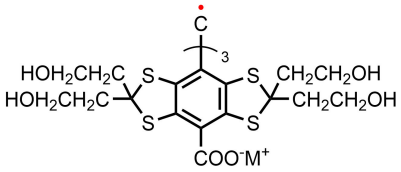

OX63

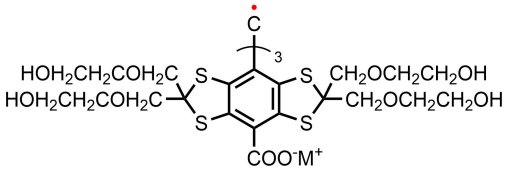

OX31

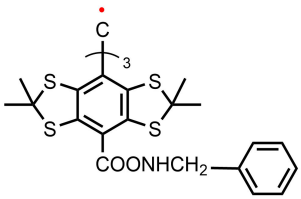

FBA_3

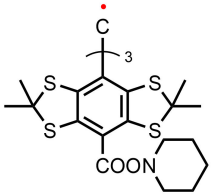

FP_3

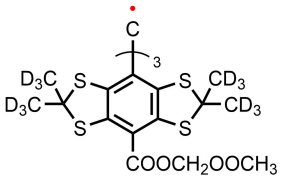

$FDAM_3$

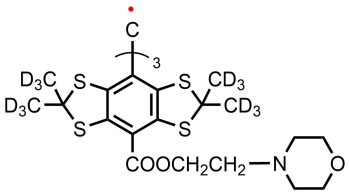

$FDME_3$

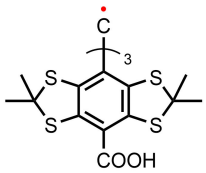

Finland trityl

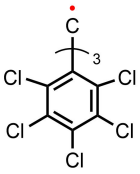

PCTM

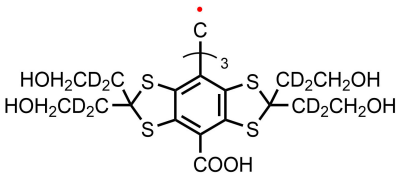

OX63D

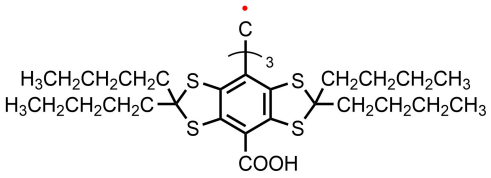

DBHT

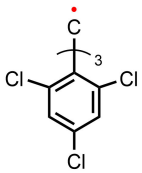

3CM

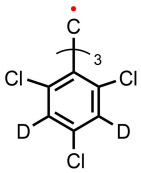

D3CM

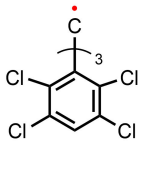

4CM

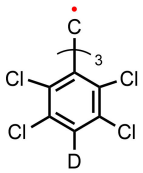

D4CM

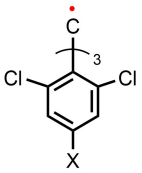

TTM-3BZ-PCL-$PDLLA_m$

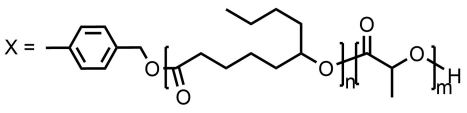

Figure S1. Schemes of triphenylmethyl radicals

Nitroxide radicals

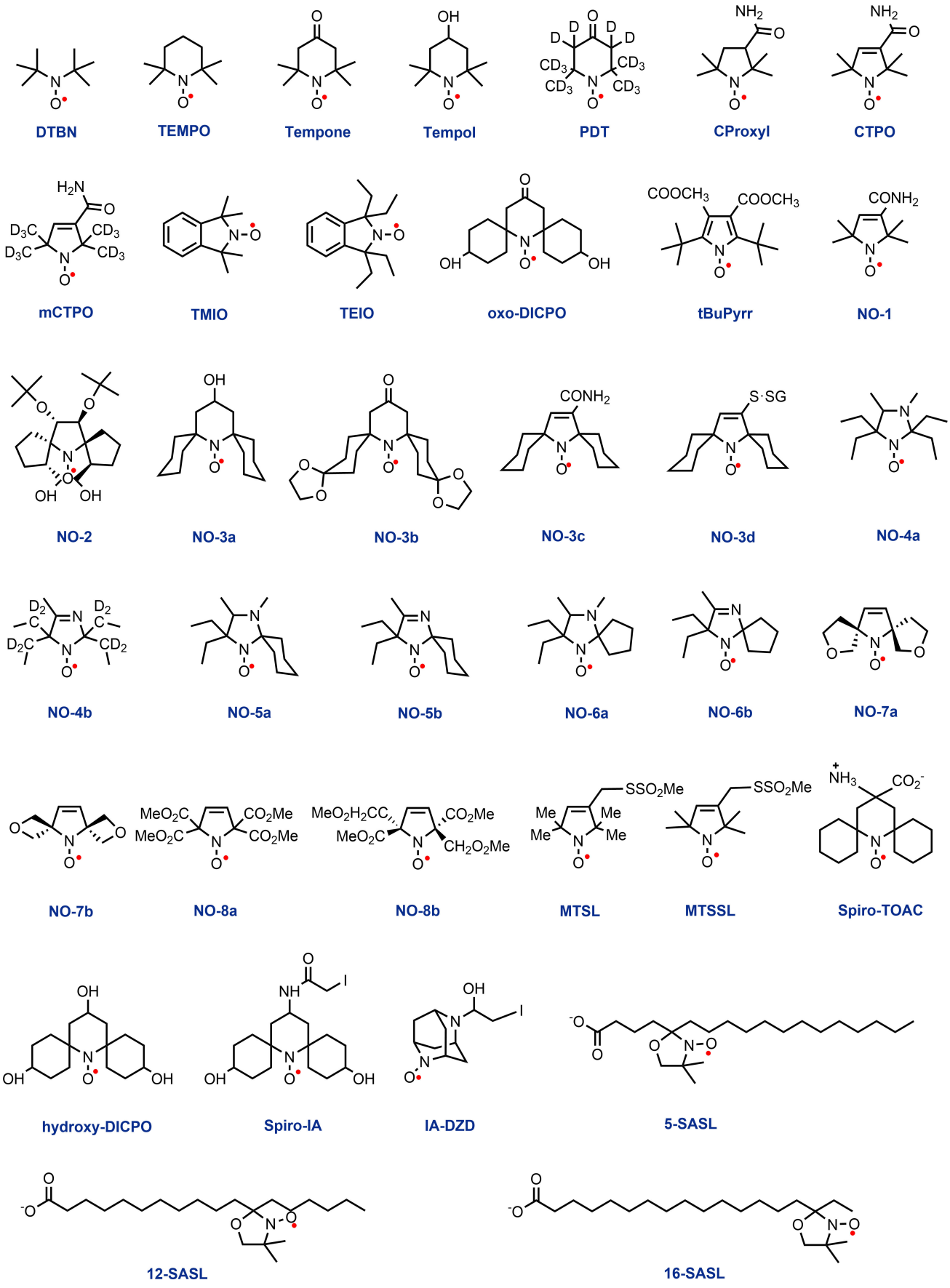

Figure S2. Schemes of nitroxide radicals

Semiquinone radicals

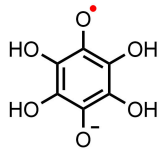

THSQ

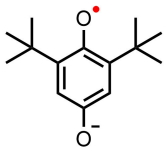

2,6-DTBSQ

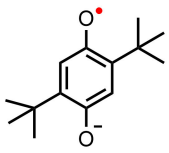

2,5-DTBSQ

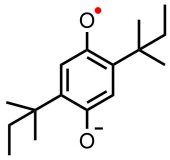

2,5-TASQ

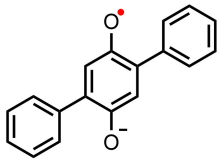

2,5-PSQ

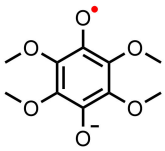

TMBSQ

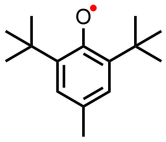

TTBP

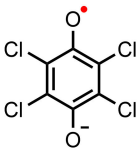

TCSQ

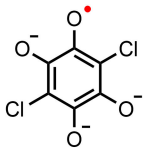

DDBSQ

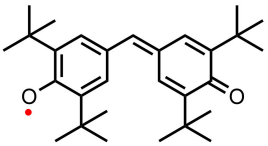

Galvinoxyl

Macrocyclic conjugated radicals

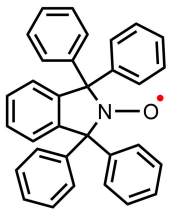

TPHIO

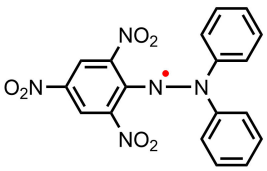

DPPH

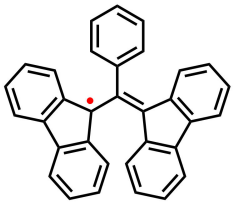

BDPA

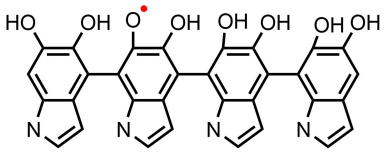

PDA

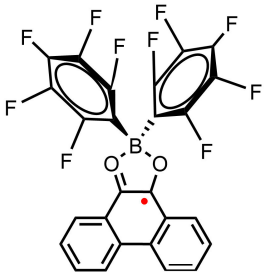

$(C_6F_5)_2B(O_2C_{14}H_8)$

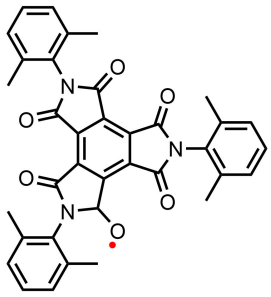

BTI-xy

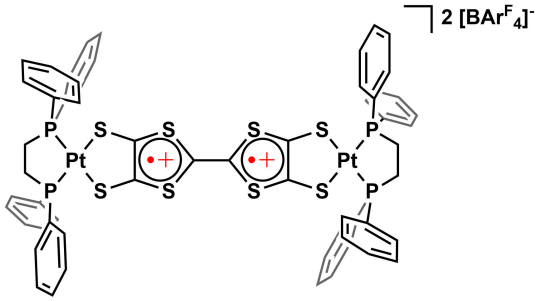

PtTTFtt

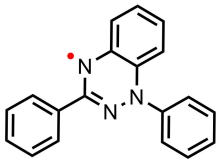

BTR

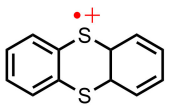

Thianthrene

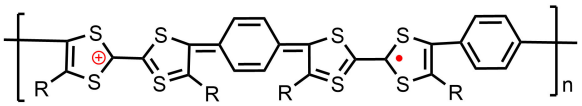

PTTF

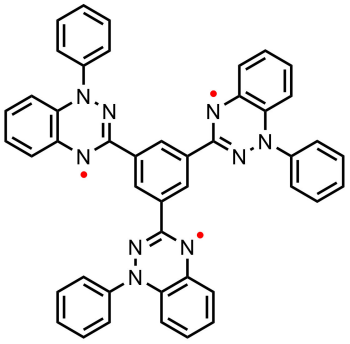

BTR-C_3

Figure S3. Scheme of semiquinone radicals and macrocyclic conjugated radicals

Graphene nanoribbons (GNRs) and carbon nanotubes

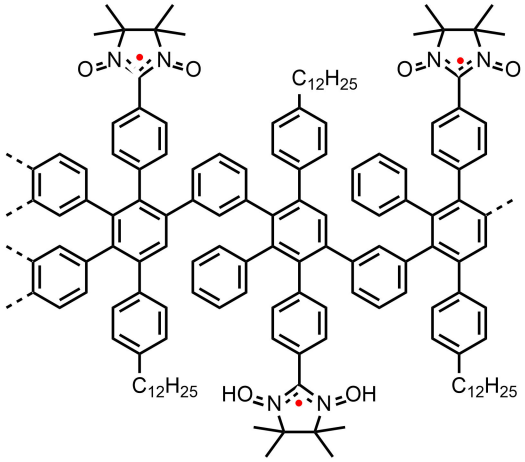

NIT-polyphenylene

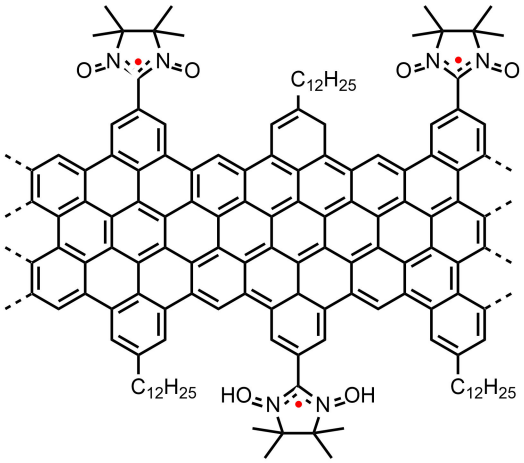

NIT-GNRs

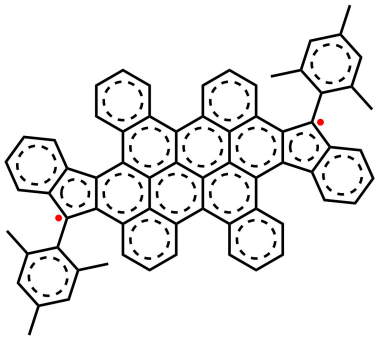

GNRs-1

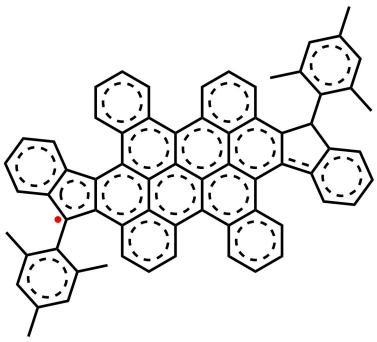

GNRs-2

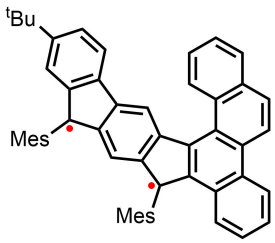

GNRs-3

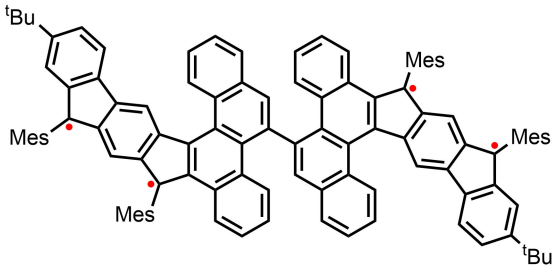

GNRs-4

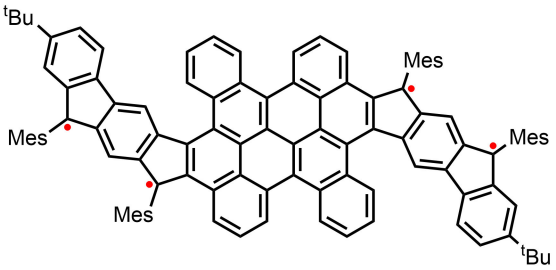

GNRs-5

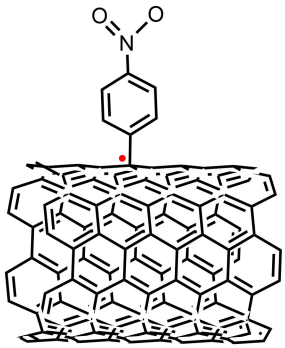

NO_2Ph-SWCNTs

Figure S4. Radicals based on graphene nanoribbons and carbon nanotubes

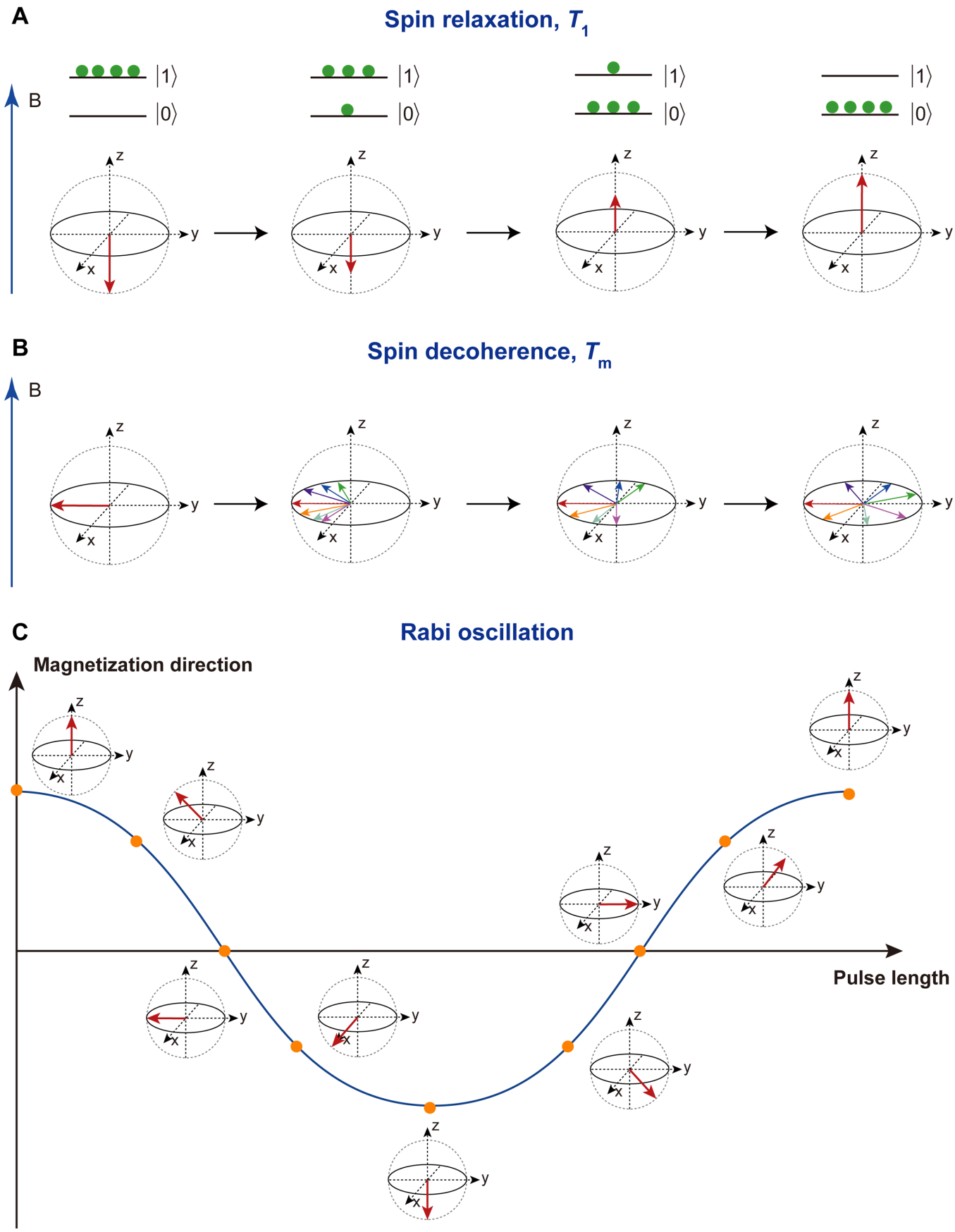

Figure S5. Bloch sphere illustrations of spin dynamics and spin manipulation (A) Spin relaxation process described by T_1. Green dots represent partitions of electron spins on $|0\rangle$ and $|1\rangle$ spin states. The blue arrow on the left marked with "B" represents the external magnetic field. (B) Spin decoherence process described by T_m. (C) Rabi oscillation.

Characterization methods for T_1, T_m, and Rabi oscillations

Radical qubit characterization, including T_1, T_m, and manipulability, relies on pulse electron paramagnetic resonance (EPR) spectroscopy. Pulse EPR spectroscopy initializes the electron spin using a static magnetic field via the Zeeman effect, manipulates it with transient oscillatory magnetic fields generated by a sequence of microwave pulses, and reads out the final state through free induction decays or spin echoes. T_1 could be measured by inversion recovery or saturation recovery pulse sequences, which transform the spin to a nonequilibrium state and monitor the relaxation process (Figure S6C, D). T_m is most often characterized by a Hahn echo decay pulse sequence that generates a superposition state and monitors its decoherence during a free evolution period (Figure S6A).[1,2] T_m may be improved by dynamical decoupling strategies that suppress the influence of environmental magnetic noise.[3,4] The manipulability is demonstrated via Rabi oscillations, which show an oscillatory relationship between superposition and the duration of a nutation pulse (Figure S5C).[5] Practically, molecules displaying quantum coherence always show Rabi oscillations in nutation experiments (Figure S6B). Thus, a radical that exhibits long T_1 and T_m could be qualified as a qubit.[1,2]

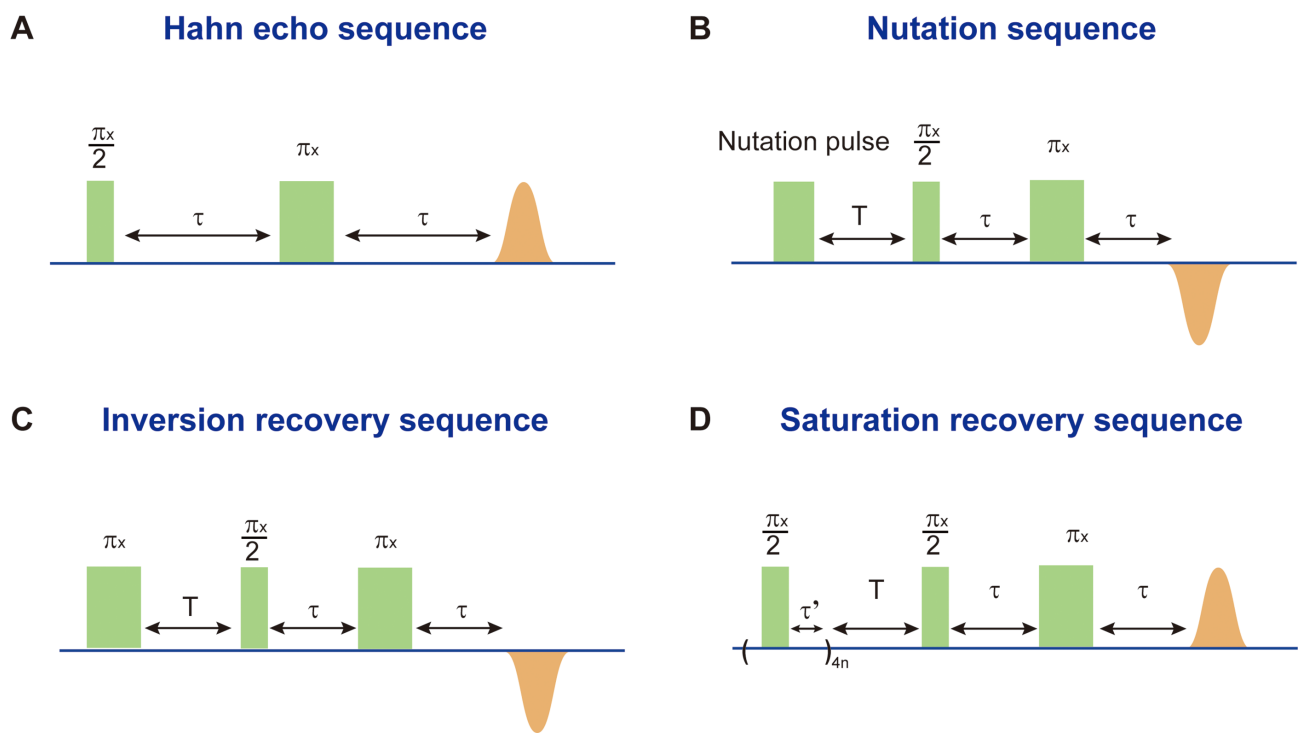

Figure S6. Schemes of pulse sequences (A) Hahn echo sequence. (B) Nutation sequence. (C) Inversion recovery sequence. (D) Saturation recovery sequence. Green rectangles represent pulses whose turning angles are marked above them, and orange objects represent spin echoes.

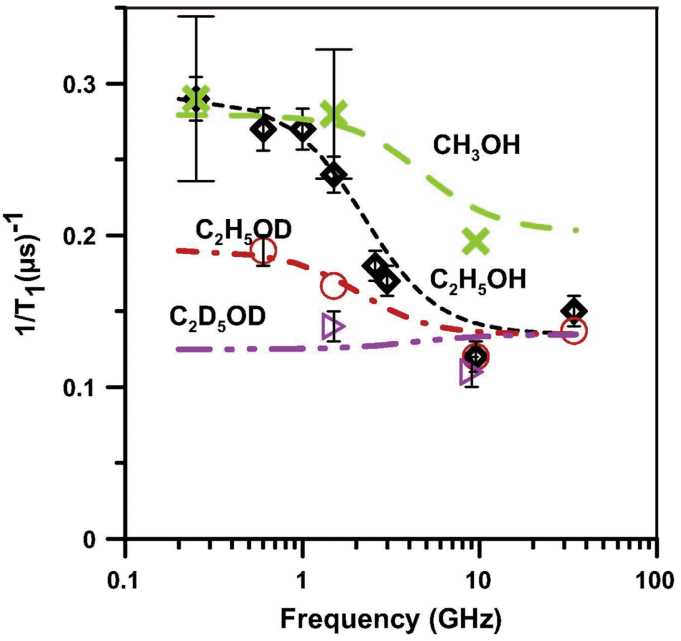

Figure S7. Influence of solvent deuteration on $1/T_1$ (Reproduced from Ref. [6] with the permission from Elsevier, copyright 2014)

Influence of the Larmor frequency on the electron spin dynamics of stable organic radical qubits

The Larmor frequency (ω) describes the frequency of spin precession in an external magnetic field (B), which reflects the Zeeman splitting (E_Z) dictated by the g-factor of spin system and the change of spin state (ΔS),

$$E_Z = \hbar\omega = g\mu_B B\Delta S$$

where $\hbar$ is the reduced Planck constant, μ_B is the Bohr magneton, and ΔS is +1 for an organic mono-radical. In typical EPR experiments, ω is fixed within a narrow range of frequency to match the resonant frequency of the microwave cavity. The resonant frequency is conventionally represented by the microwave band of the EPR instrument, with L-band centered at 1 GHz, S-band 3.5 GHz, X-band 9.8 GHz, Q-band 34 GHz, and W-band 94 GHz.

Electron spins with different Larmor frequencies might couple with different phonon modes, which in turn affects spin relaxation processes. Raman, Orbach, and local-mode processes typically involve phonons whose frequencies are well above the Larmor frequency of spin, so these processes are frequency-independent.[1,2] In contrast, direct and thermally activated processes that involve low-frequency phonons typically show significant frequency dependence. The former monotonically increases with rising Larmor frequency, whereas the latter has a maximum value that appears when $\omega\tau_c = 1$ where τ_c is the correlation time of the thermally activated process.[7,8] For example, for a nitroxide radical, PDT (Figure S2), dissolved in a mixture of water and glycerol, $\tau_c = 1.0 \times 10^{-10}\ s$. Hence, the thermally activated process is the most pronounced at the frequency $\nu = \frac{\omega}{2\pi} = 1.6\ GHz$. This is in good agreement with the experimental observation where $1/T_1$ shows the maximum at 1.5 GHz (Figure S8B).[7]

As discussed in the main text, spin relaxation processes in fluid solution mainly include tumbling-induced spin rotation and modulation of anisotropic interactions comprising of g-anisotropy, A-anisotropy, and dipolar coupling with solvent nuclei.[1] According to the corresponding equation in Table S1, the spin rotation is independent of the Larmor frequency (Figure 5A), yet others are frequency-dependent (Figure 5B–D) and their salience is related to the tumbling correlation time (τ_R). For instance, Biller et al. acquired the room-temperature T_1 of a series of nitroxide radicals at various frequencies (250 MHz to 34 GHz) in solutions whose τ_R values range from 4 to 50 ps.[8] Take the PDT radical (Figure S2) as an example. When τ_R is 4 ps, the spin relaxation is predominantly governed by spin rotation, rendering T_1 independent of frequency (T_1 = 1.05 − 1.18 μs; Figure S8A). In contrast, as τ_R exceeds 15 ps, the dominant process shifts towards g- and A-anisotropy modulations. Meanwhile, the thermally activated process exerts its most substantial influence on T_1 within the frequency range of 1 − 2 GHz. Consequently, as τ_R increases, the frequency-dependence of T_1 becomes more and more salient. For example, when τ_R is 50 ps, T_1 drops from approximately 4.5 μs at 250 MHz to approximately 0.28 μs at 34 GHz.[7]

The frequency-dependence of T_m remains unclear. Shi *et al* found that the T_m of triphenylmethyl radicals only shows weak frequency-dependence within the range of 250 MHz – 1.5 GHz.[9] Biller *et al* showed that nitroxide radicals exhibit decreasing T_m with increasing frequency from 250 MHz to 34 GHz.[7] In contrast, Ghim *et al* observed that within the range of 1.8 – 19.4 GHz, the T_m of irradiated L- alanine radicals increases with increasing frequency.[10] From these observations, it seems that the frequency dependence of T_m may be different for different radicals and/or frequency ranges. A comprehensive and in-depth investigation into this phenomenon is needed.

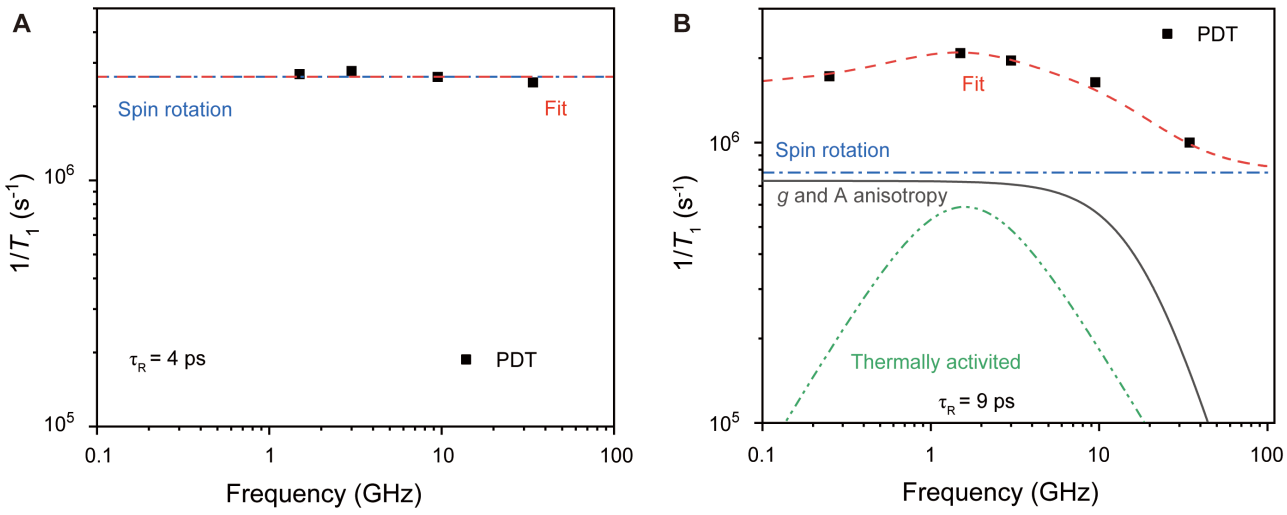

Figure S8. Influence of Larmor frequency on spin dynamics Frequency dependence of $1/T_1$ for PDT in solvents whose τ_R being (A) 4 ps and (B) 9 ps, respectively. Data used for these two simulations (black squares) are extracted from Ref[8] for (A) and Ref[7] for (B).

Table S1. The equation of typical spin relaxation mechanisms[1,11,12]

Mechanism	Equation
Direct	$A_{Dir}B^4\frac{e^{\hbar\omega/k_BT}}{e^{\hbar\omega/k_BT}-1}$
Raman	$A_{Ram}\left(\frac{T}{\Theta_D}\right)^9\int_0^{\frac{\Theta_D}{T}}x^8\frac{e^x}{(e^x-1)^2}dx$ (sometimes $A_{Ram}T^m$ with $m=2-9$)
Orbach	$A_{Orb}\frac{\Delta^3}{e^{\Delta/k_BT}-1}$
Local mode	$A_{loc}\frac{e^{\hbar\omega_{phonon}/k_BT}}{\left(e^{\hbar\omega_{phonon}/k_BT}-1\right)^2}$
Thermally activated	$A_{therm}\frac{2\tau_c^0e^{E_a/k_BT}}{1+\omega^2{\tau_c^0}^2e^{2E_a/k_BT}}$
Tumbling-dependent	$\frac{\sum_{i=x,y,z}(g_i-g_e)^2}{9\tau_R}+\frac{2}{5}\left(\frac{\mu_B\omega}{g\beta}\right)^2\left\{\frac{(\Delta g)^2}{3}+(\delta g)^2\right\}J(\omega)$ $+\frac{2}{9}I(I+1)\sum_i(A_i-a_{iso})^2J(\omega)+C_{solvent}\frac{\tau_{solvent}}{1+(\omega\tau_{solvent})^2}$
Cross relaxation	constant (temperature-independent)

T: temperature; B: magnetic field strength; ω: Larmor frequency; Θ_D: Debye temperature; Δ: energy of low-lying excited state; ω_{phonon}: energy of local phonon mode. τ_c^0: pre-exponential factor; E_a: activation energy; g_i: principle *g* value along the *i* axis; g_e: *g* value of free electron; τ_R: tumbling correlation time; μ_B: Bohr magneton; $\Delta g = g_{zz} - 0.5(g_{xx}+g_{yy})$; $\delta g = 0.5(g_{xx}-g_{yy})$; $J(\omega)=\frac{\tau_R}{1+(\omega\tau_R)^2}$; I: nuclear spin; A_i: principle component of the nuclear hyperfine constant along the *i* axis in angular frequency units; a_{iso}: the isotropic nuclear hyperfine constant; $\tau_{solvent}$: correlation time for motion of the solvent relative to the radical; $C_{solvent}$: a function of the dipolar interaction with solvent nuclei. A_{Dir}, A_{Ram}, A_{Orb}, A_{loc}, A_{therm} are pre-factors.

Table S2. T_1 and T_m of stable organic radical qubits

Radical[a]	Concentration / mmol·L^{-1}	Frequency / GHz	Solvent	Temperature / K	T_1 / μs	T_m / μs	Reference
Trityl-CH_3	0.2	9.5	H_2O : glycerol = 1:1	100	1060	3.9	[13]
				294	16	2.2	[14]
			H_2O : glycerol = 1:9	294	17	0.18	
			H_2O	294	15	8.7	
		95	H_2O : glycerol = 1:1	100	838	3.1	[13]
Trityl-CD_3	0.2	9.5	H_2O : glycerol = 1:1	100	955	4.8	[13]
				294	17	3.7	[14]
			H_2O : glycerol = 1:9	294	19	0.24	
			H_2O	294	17	11	
		95	H_2O : glycerol = 1:1	100	756	4.5	[13]
		1.5	H_2O : glycerol = 1:1	294	15	4.2	[14]
			H_2O : glycerol = 1:9	294	18	0.21	
			H_2O	294	14	12.5	
		3.1	H_2O : glycerol = 1:1	294	16	3.8	
			H_2O	294	16	13	
Finland trityl	2.5	9.5	H_2O : glycerol = 4:6	77	1670[b]	NA[c]	[15]
		95			1100[b]		
OX63	0.2	9.5	H_2O : glycerol = 1:1	100	1200	5.1	[13]
		95			979	4.5	[13]
OX31	0.2	9.5	H_2O : glycerol = 1:1	100	1360	5.0	[13]
		95			1042	4.4	[13]
$FDAM_1$	NA[c]	9.5	MeOH	300	14.3	7.6	[16]
		34			12.6	2.8	
		9.5	H_2O	300	14.5	10.1	
		34			NA[c]	4.7	
$FDAM_2$	NA[c]	9.5	MeOH	300	11.6	8.1	[16]
		34			11.6	4.9	
		9.5	CH_2Cl_2	300	12.3	9.6	
		34			11.3	6.7	
		9.5	$CHCl_3$	300	11.0	8.6	
		34			10.0	5.6	
		9.5	CH_2ClCH_2Cl	300	10.5	6.0	
		34			10.3	4.3	
		9.5	CH_3CH_2OH	300	10.1	6.0	
		34			10.0	3.1	
		9.5	Tert-butanol	300	11.7	4.0	
		34			12.2	1.4	
$FDAM_3$	NA[c]	9.5	MeOH	300	11.1	8.3	[16]
		34			9.7	5.6	
		9.5	$CHCl_3$	300	9.9	8.4	
		34			9.6	6.0	
OX63D	1	9.5	H_2O : glycerol = 4:6	77	3334[b]	NA[c]	[15]
		95			5000[b]		
OX63D	NA[c]	9.5	MeOH	300	16.5	5.8	[16]
		34			15.6	1.8	
		9.5	H_2O	300	16.0	7.3	
		34			15.3	2.2	
		9.5	D_2O	300	16.1	7.6	
		34			16.1	2.0	
DBT	NA[c]	9.5	MeOH	300	14.9	5	[16]
		34			14.3	2.1	

FBA_3	NA[c]	9.5	MeOH	300	19.5	6.5	16
		34			19.2	3.6	
		9.5	$CHCl_3$	300	18.0	7.2	
		34			17.6	4.5	
FP_3	NA[c]	9.5	MeOH	300	23.0	5.0	16
		34			23.0	2.8	
		9.5	$CHCl_3$	300	26.4	4.5	
		34			25.7	2.3	
$FDME_3$	NA[c]	9.5	MeOH	300	12.2	8.5	16
		34			11.2	5.4	
		9.5	$CHCl_3$	300	11.4	9.1	
		34			11.2	5.4	
BDPA	0.0007	9.5	Toluene	Ambient temperature	12[b]	9.8[b]	17
DPPH	0.012	9.5	Toluene	Ambient temperature	2.0[b]	1.3[b]	17
Galvinoxyl	0.0028	9.5	Toluene	Ambient temperature	2.8[b]	2.1[b]	17
Thianthrene	< 0.5	9.5	TFA	Ambient temperature	0.4[b]	0.4[b]	17
mCTPO	0.25	9.5	H_2O	Ambient temperature	0.53	0.67	17
PDT	0.25	9.5	H_2O	Ambient temperature	0.56	0.59	17
2,5-DTBSQ	0.3	9.5	Ethanol	Ambient temperature	7.8[b]	3.2[b]	6
2,6-DTBSQ	0.3	9.5	Ethanol	Ambient temperature	6.67[b]	NA[c]	
TMBSQ	0.3	9.5	Ethanol	Ambient temperature	5.56[b]		
TEMPO	1.0	9.5	H_2O: glycerol = 1:1	295[b]	2.00[b]	NA[c]	18
Tempone	0.3	9.5	H_2O: glycerol = 1:1	100	100[b]	5[b]	19
Tempol	3	9.5	Sucrose octaacetate	298[b]	19.95[b]	NA[c]	20
DTBN	3	9.5	Sucrose octaacetate	250[b]	5.6[b]	0.40[b]	
TEIO	3	9.5	Sucrose octaacetate	300[b]	25.12[b]	0.63[b]	
TMIO	3	9.5	Sucrose octaacetate	300[b]	NA[c]	1.26[b]	
TPHIO	3	9.5	Sucrose octaacetate	298[b]	56.23[b]	2.51[b]	
CTPO	3	9.5	Sucrose octaacetate	273[b]	15.85[b]	1.58	
tBuPyrr	3	9.5	Sucrose octaacetate	273[b]	NA[c]	0.63	
PCTM	0.2-0.5	9.5	Toluene : $CHCl_3$ = 4:1	298	10[b]	NA[c]	21
TCSQ	0.2-0.5	9.5	Triacetin : HMPA = 2:1	298	10[b]		
DDBSQ	0.2-0.5	9.5	H_2O : glycerol = 1:1	298	31.63[b]		
TTBP	0.53	9.1	H_2O : glycerol = 1:1	298	10[b]	NA[c]	22
THSQ	0.5	9.5	Ethanol : glycerol = 4:1	298	31.63[b]	NA[c]	23
2,5-TASQ	0.5	9.5	Ethanol : glycerol = 4:1	298	10[b]		
2,5-PSQ	0.5	9.5	Ethanol : glycerol = 4:1	298	10[b]		
PTTF	powder	NA[c]	NA[c]	300[b]	1[b]	0.5[b]	24
PtTTFtt	0.05	9.5	DCM	298	1.44[b]	0.34[b]	25
$(C_6F_5)_2B(O_2C_{14}H_8)$	0.1	9.5	Toluene : CH_2Cl_2 = 9:1	100	4600	2.6	26
BTI-xy	0.2	9.5	DMF : benzene = 1:1	10	6000[b]	1.3[b]	27
BTR-C_3	1	9.5	2-Methyltetrahydrofuran	5	1098	6.8	28
				110	23	2.8	
PDA	NA[c]	9.5	powder	5	46900	0.77	29
hydroxyl-DICPO	NA[c]	9.5	H_2O : glycerol = 1:1	100	400[b]	3.2[b]	30
oxo-DICPO	NA[c]	9.5	H_2O : glycerol = 1:1	100	400[b]	3.2[b]	
IA-DZD	NA[c]	35	H_2O : glycerol = 1:1	80	580	2.7	31
NO-1	NA[c]	9.5	Dried trehalose	Room temperature	12	0.735	32
NO-2					30	0.730	
NO-3a					17	0.750	

NO-3b					17	0.730	
NO-3c					21	0.8	
NO-3d					22	0.630	
NO-4a					18	0.680	
NO-4b					14	0.650	
NO-5a					18	0.640	
NO-5b					16	0.740	
NO-6a					23	0.655	
NO-6b					16	0.730	
NO-7a	NA[c]	9.5	Trehalose : sucrose = 9:1	Room temperature	NA[c]	0.50[b]	33
NO-7b						0.71[b]	
MTSL						0.34[b]	
NO-8a	NA[c]		Trehalose : sucrose = 9:1	295[b]	10[b]	1[b]	34
NO-8b	NA[c]		Trehalose :sucrose = 9:1	295[b]	10[b]	1[b]	
MTSSL	NA[c]	9.5	H_2O : glycerol = 1:1	240[b]	10[b]	0.1[b]	35
				100[b]	400[b]	1[b]	
Spiro-TOAC	NA[c]	9.5	H2O : glycerol = 1:1	240	NA[c]	0.1[b]	
				100		3.2[b]	
Spiro-IA	NA[c]	9.5	H_2O : glycerol = 1:1	100	NA[c]	3.16[b]	36
5-SASL	NA[c]	2.54	DMPC	300	1.34	NA[c]	37
		3.45			2.06		
		9.2			5.33		
		18.5			6.98		
		34.6			8.41		
12-SASL	NA[c]	2.54	DMPC	300	1.18	NA[c]	37
		3.45			1.67		
		9.2			4.41		
		18.5			5.81		
		34.6			6.11		
16-SASL	NA[c]	2.54	DMPC	300	0.69	NA[c]	37
		3.45			0.92		
		9.2			2.52		
		18.5			3.46		
		34.6			3.69		
NIT-polyphenylene	NA[c]	9.4	Powder	300[b]	1.43[b]	0.6[b]	38
NIT-GNRs					1.43[b]	0.2[b]	
GNRs-1	NA[c]	9.8	Powder	Room temperature	1[b]	0.3[b]	39
				5	100[b]	NA[c]	
			Toluene	5	5000[b]	2[b]	
			d-Toluene	5	10000[b]	NA[c]	
			CS_2	80[b]	NA[c]	100[b]	
GNRs-2	NA[c]	9.8	d-Toluene	15[b]	NA[c]	10[b]	39
			CS_2	10[b]		20[b]	
GNRs-3	NA[c]	9.4	Powder	10[b]	NA[c]	1[b]	40
	2±0.5		Toluene	300[b]	100[b]	6[b]	
	2±0.5		d-Toluene		83[b]	6[b]	
	2±0.5		CS_2		83[b]	7[b]	
	2±0.5		d_{14}OTP		1000[b]	6[b]	
GNRs-4	NA[c]	9.4	Powder	10[b]	NA[c]	0.2[b]	40
	2±0.5		Toluene	300[b]	125[b]	4[b]	
	2±0.5		d-Toluene		100[b]	3[b]	

	2±0.5		CS_2		100[b]	4[b]	
	2±0.5		d_{14}OTP		1000[b]	2[b]	
GNRs-5	NA[c]	9.4	Powder	10[b]	NA[c]	0.1[b]	40
	2±0.5		Toluene	300[b]	91[b]	5[b]	
	2±0.5		d-Toluene		250[b]	5[b]	
	2±0.5		CS_2		67[b]	5[b]	
	2±0.5		d_{14}OTP		1000[b]	3[b]	
NO2Ph-SWCNTs	NA[c]	9.5	d-Toluene	5	13000	1.2	41
D3CM	NA[c]	9.26	Powder	100[b]	800[b]	1[b]	42
				298[b]	20[b]	1[b]	
	0.1		d^8-Toluene	100[b]	1000[b]	4[b]	
3CM	NA[c]		Powder	100[b]	600[b]	0.7[b]	
				298[b]	15[b]	0.7[b]	
	0.1		d^8-Toluene	100[b]	1000[b]	2[b]	
D4CM	NA[c]		Powder	100[b]	300[b]	0.8[b]	
				298[b]	60[b]	0.6[b]	
	0.1		d^8-Toluene	100[b]	800[b]	4[b]	
4CM	NA[c]		Powder	100[b]	200[b]	0.2[b]	
	0.1		d^8-Toluene	100[b]	1000[b]	1[b]	

[a]Abbreviations are consistent with those in Figure S1-4; [b]value estimated from a figure in the reference; [c]not available.

Table S3. T_1 and T_m of stable organic radical qubits integrated in solid-state systems

Radical[a]	Molar percentage	Frequency / GHz	Temperature / K	T_1 / μs	T_m / μs	Reference
C_{50}-LA_{90}	1%[e]	9.73	30	2102	0.186	43
		9.65	298	25.02	0.148	
C_{50}-LA_{140}	0.7%[e]	9.73	30	3522	0.300	
		9.65	298	29.62	0.213	
C_{50}-LA_{400}	0.4%[e]	9.73	30	5173	0.377	
		9.65	298	29.23	0.318	
MgHOTP	0.66%	9.4	296	10.55	0.153	44
			296	21.61[b]	0.202[b]	
TAPPy-NDI	0.01%	9.4	100	790	1.26	45
			296	30.2	0.49	
	0.11%		100	333	0.727	
			296	11.8	0.484	
	2.1%		100	357	0.702	
			296	15	0.397	
	8.2%		100	257	0.448	
			296	11	0.283	
	15%		100	92.7	0.216	
			296	7.7	0.108	
	32%		100	30.6	0.166	
			296	1.68	0.150	
Ni-HATI_iPr	1%	9.7	100	3[c]	0.09[c]	46
Ni-HATI_vPr	0.3%	9.7	50	8[c]	0.08[c]	
Ni-HATI_nPr	0.4%	9.7	100	2[c]	0.07[c]	
PTCM-Film	0.1%	9.26	100	150[c]	1.5[c]	42
			298	35.6	1.08	
TEMPO SAM	N/A[d]	9.47	10	9200	13.53	47
BTEV-BTR	1%	9	80	386	4.39	48
			293	36	2.30	
	5%		293	29	1.73	
	10%		293	26	1.43	
	20%		80	75	1.86	
			293	20	0.98	

[a]Abbreviations are consistent with those in corresponding references; [b]MgHOTP soaked in THF; [c]value estimated from a figure in the reference; [d]not available; [e]value estimated from the synthetic condition.

References

1. Eaton, S.S., Eaton, G.R. (2018) Relaxation mechanisms. In EPR Spectroscopy: Fundamentals and Methods, Goldfarb, D., Stoll, S., ed. (Wiley), pp. 175–192.

2. Eaton, S.S., Eaton, G.R. (2000) Relaxation times of organic radicals and transition metal ions. In Distance Measurements in Biological Systems by EPR, Berliner, L. J., Eaton, G.R., Eaton, S.S., ed. (Kluwer Academic/Plenum Publishers), pp. 29–154.

3. Mirzoyan, R., Kazmierczak, N.P., Hadt, R.G. (2021). Deconvolving contributions to decoherence in molecular electron spin qubits: a dynamic ligand field approach. Chem. Eur. J. **27**: 9482–9494. DOI: 10.1002/chem.202100845.

4. Bhattacharyya, R., Chakraborty, I., Chakrabarti, A., et al. (2020). Recent studies on accurate measurements of NMR transverse relaxation times. Annu. Rep. NMR Spectrosc. **99**: 57–77. DOI: 10.1016/bs.arnmr.2019.09.001

5. Atzori, M., Sessoli, R. (2019). The second quantum revolution: role and challenges of molecular chemistry. J. Am. Chem. Soc. **141**: 11339–11352. DOI: 10.1021/jacs.9b00984.

6. Elajaili, H.B., Biller, J.R., Eaton, S.S., et al. (2014). Frequency dependence of electron spin–lattice relaxation for semiquinones in alcohol solutions. J. Magn. Reson. **247**: 81–87. DOI: 10.1016/j.jmr.2014.08.014.

7. Biller, J.R., Meyer, V.M., Elajaili, H., et al. (2012). Frequency dependence of electron spin relaxation times in aqueous solution for a nitronyl nitroxide radical and perdeuterated-tempone between 250 MHz and 34 GHz. J. Magn. Reson. **225**: 52–57. DOI: 10.1016/j.jmr.2012.10.002.

8. Biller, J.R., Elajaili, H., Meyer, V., et al. (2013). Electron spin–lattice relaxation mechanisms of rapidly-tumbling nitroxide radicals. J. Magn. Reson. **236**: 47–56. DOI: 10.1016/j.jmr.2013.08.006.

9. Shi, Y., Quine, R.W., Rinard, G.A., et al. (2017). Triarylmethyl radical: EPR signal to noise at frequencies between 250 MHz and 1.5 GHz and dependence of relaxation on radical and salt concentration and on frequency. Z. Für Phys. Chem. **231**: 923–937. DOI: 10.1515/zpch-2016-0813.

10. Ghim, B.T., Du, J.-L., Pfenninger, S., et al. (1996). Multifrequency electron paramagnetic resonance of irradiated L-alanine. Appl. Radiat. Isot. **47**: 1235–1239. DOI: 10.1016/s0969-8043(96)00037-1.

11. Kevan, L., Narayana, P.A. (1979) Disordered matrices. In Multiple Electron Resonance Spectroscopy, Dorio, M.M., Freed, J.H., ed. (Plenum Press), pp. 229–260.

12. Bowman, M.K., Norris, J.R. (1982). Cross relaxation of free radicals in partially ordered solids. J. Phys. Chem. **86**: 3385–3390. DOI: 10.1021/j100214a024.

13. Fielding, A.J., Carl, P.J., Eaton, G.R., et al. (2005). Multifrequency EPR of four triarylmethyl radicals. Appl. Magn. Reson. **28**: 231–238. DOI: 10.1007/BF03166758.

14. Yong, L., Harbridge, J., Quine, R.W., et al. (2001). Electron spin relaxation of triarylmethyl radicals in fluid solution. J. Magn. Reson. **152**: 156–161. DOI: 10.1006/jmre.2001.2379.

15. Chen, H., Maryasov, A.G., Rogozhnikova, O. Y., et al. (2016). Electron spin dynamics and spin–lattice relaxation of trityl radicals in frozen solutions. Phys. Chem. Chem. Phys. **18**: 24954–24965. DOI: 10.1039/c6cp02649d.

16. Kuzhelev, A.A., Trukhin, D.V., Krumkacheva, O.A., et al. (2015). Room-temperature electron spin relaxation of triarylmethyl radicals at the X- and Q- bands. J. Phys. Chem. B **119**: 13630–13640. DOI: 10.1021/acs.jpcb.5b03027.

17. Meyer, V., Eaton, S.S., Eaton, G.R. (2014). X-band electron spin relaxation times for four aromatic radicals in fluid solution and comparison with other organic radicals. Appl. Magn. Reson. **45**: 993–1007. DOI: 10.1007/s00723-014-0579-6.

18. Sato, H., Bottle, S.E., Blinco, J.P., et al. (2008). Electron spin–lattice relaxation of nitroxyl radicals in temperature ranges that span glassy solutions to low-viscosity liquids. J. Magn. Reson. **191**: 66–77. DOI: 10.1016/j.jmr.2007.12.003.

19. Nakagawa, K., Candelaria, M.B., Chik, W.W.C., et al. (1992). Electron-spin relaxation times of chromium(V). J. Magn. Reson. **98**: 81–91. DOI: 10.1016/0022-2364(92)90111-J.

20. Sato, H., Kathirvelu, V., Fielding, A., et al. (2007). Impact of molecular size on electron spin relaxation rates of nitroxyl radicals in glassy solvents between 100 and 300 K. Mol. Phys. **105**: 2137–2151. DOI: 10.1080/00268970701724966.

21. Kathirvelu, V., Eaton, G.R., Eaton, S.S. (2009). Impact of chlorine substitution on spin–lattice relaxation of triarylmethyl and 1,4-benzosemiquinone radicals in glass-forming solvents between 25 and 295 K. Appl. Magn. Reson. **37**: 649. DOI: 10.1007/s00723-009-0086-3.

22. Harbridge, J.R., Eaton, S.S., Eaton, G.R. (2003). Electron spin-lattice relaxation processes of radicals in irradiated crystalline organic compounds. J. Phys. Chem. **107**: 598–610. DOI: 10.1021/jp021504h.

23. Kathirvelu, V., Sato, H., Eaton, S.S., et al. (2009). Electron spin relaxation rates for semiquinones between 25 and 295 K in glass-forming solvents. J. Magn. Reson. **198**: 111–120. DOI: 10.1016/j.jmr.2009.01.026.

24. Krinichnyi, V.I., Pelekh, A.E., Roth, H.-K., et al. (1993). Spin relaxation studies on conducting poly(tetrathiafulvalene). Appl. Magn. Reson. **4**: 345–356. DOI: 10.1007/BF03162508.

25. McNamara, L., Zhou, A., Rajh, T., et al. (2023). Realizing solution-phase room temperature quantum coherence in a tetrathiafulvalene-based diradicaloid complex. Cell Rep. Phys. Sci. **4**: 101693. DOI: 10.1016/j.xcrp.2023.101693.

26. Eaton, S.S., Huber, K., Elajaili, H., et al. (2017). Electron spin relaxation of a boron-containing heterocyclic radical. J. Magn. Reson. **276**: 7–13. DOI: 10.1016/j.jmr.2016.12.013.

27. Koyama, S., Sato, K., Yamashita, M., et al. (2023). Observation of slow magnetic relaxation phenomena in spatially isolated π-radical ions. Phys. Chem. Chem. Phys. **25**: 5459–5467. DOI: 10.1039/d2cp06026d.

28. Boudalis, A.K., Constantinides, C.P., Chrysochos, N., et al. (2023). Deciphering the ground state of a C_3-symmetrical Blatter-type triradical by CW and pulse EPR spectroscopy. J. Magn. Reson. **349**: 107406. DOI: 10.1016/j.jmr.2023.107406.

29. Tadyszak, K., Mrówczyński, R., Carmieli, R. (2021). Electron spin relaxation studies of polydopamine radicals. J. Phys. Chem. B **125**: 841–849. DOI: 10.1021/acs.jpcb.0c10485.

30. Kathirvelu, V., Smith, C., Parks, C., et al. (2009). Relaxation rates for spirocyclohexyl nitroxyl radicals are suitable for interspin distance measurements at temperatures up to about 125 K. Chem. Commun., 454–456. DOI: 10.1039/b817758a.

31. Yang, Z., Stein, R.A., Ngendahimana, T., et al. (2020). Supramolecular approach to electron paramagnetic resonance distance measurement of spin-labeled proteins. J. Phys. Chem. B **124**: 3291–3299. DOI: 10.1021/acs.jpcb.0c00743.

32. Kuzhelev, A.A., Strizhakov, R.K., Krumkacheva, O.A., et al. (2016). Room-temperature electron spin relaxation of nitroxides immobilized in trehalose: effect of substituents adjacent to no-group. J. Magn. Reson. **266**: 1–7. DOI: 10.1016/j.jmr.2016.02.014.

33. Huang, S., Pink, M., Ngendahimana, T., et al. (2021). Bis-spiro-oxetane and bis-spiro-tetrahydrofuran pyrroline nitroxide radicals: synthesis and electron spin relaxation studies. J. Org. Chem. **86**: 13636–13643. DOI: 10.1021/acs.joc.1c01670.

34. Huang, S., Paletta, J.T., Elajaili, H., et al. (2017). Synthesis and electron spin relaxation of tetracarboxylate pyrroline nitroxides. J. Org. Chem. **82**: 1538–1544. DOI: 10.1021/acs.joc.6b02737.

35. Rajca, A., Kathirvelu, V., Roy, S.K., et al. (2010). A spirocyclohexyl nitroxide amino acid spin label for pulsed EPR spectroscopy distance measurements. Chem. Eur. J. **16**: 5778–5782. DOI: 10.1002/chem.200903102.

36. Meyer, V., Swanson, M.A., Clouston, L.J., et al. (2015). Room-Temperature distance measurements of immobilized spin-labeled protein by DEER/PELDOR. Biophys. J. **108**: 1213–1219. DOI: 10.1016/j.bpj.2015.01.015.

37. Hyde, J.S., Yin, J.-J., Subczynski, W.K., et al. (2004). Spin-label EPR T_1 values using saturation recovery from 2 to 35 GHz. J. Phys. Chem. B **108**: 9524–9529. DOI: 10.1021/jp036329z.

38. Slota, M., Keerthi, A., Myers, W.K., et al. (2018). Magnetic edge states and coherent manipulation of graphene nanoribbons. Nature **557**: 691–695. DOI: 10.1038/s41586-018-0154-7.

39. Lombardi, F., Lodi, A., Ma, J., et al. (2019). Quantum units from the topological engineering of molecular graphenoids. Science **366**: 1107–1110. DOI: 10.1126/science.aay7203.

40. Lombardi, F., Ma, J., Alexandropoulos, D.I., et al. (2021). Synthetic tuning of the quantum properties of open-shell radicaloids. Chem **7**: 1363–1378. DOI: 10.1016/j.chempr.2021.03.024.

44. Chen, J.-S., Trerayapiwat, K.J., Sun, L., et al. (2023). Long-lived electronic spin qubits in single-walled carbon nanotubes. Nat. Commun. **14**: 848. DOI: 10.1038/s41467-023-36031-z.

42. Dai, Y., Dong, B., Kao, Y., et al. (2018). Chemical modification toward long spin lifetimes in organic conjugated radicals. ChemPhysChem **19**: 2972–2977. DOI: 10.1002/cphc.201800742

43. Hou, L., Zhang, Y., Zhang, Y., et al. (2024). Tunable quantum coherence of luminescent molecular spins organized via block copolymer self-assembly. Adv. Quantum Technol. 2400064. DOI: 10.1002/qute.202400064

44. Sun, L., Yang, L., Dou, J.-H., et al. (2022). Room-temperature quantitative quantum sensing of lithium ions with a radical-embedded metal–organic framework. J. Am. Chem. Soc. **144**: 19008–19016. DOI: 10.1021/jacs.2c07692.

45. Oanta, A.K., Collins, K.A., Evans, A.M., et al. (2023). Electronic spin qubit candidates arrayed within layered two-dimensional polymers. J. Am. Chem. Soc. **145**: 689–696. DOI: 10.1021/jacs.2c11784.

46. Lu, Y., Hu, Z., Petkov, P., et al. (2024). Tunable charge transport and spin dynamics in two-dimensional conjugated metal–organic frameworks. J. Am. Chem. Soc. **146**: 2574–2582. DOI: 10.1021/jacs.3c11172.

47. Tesi, L., Stemmler, F., Winkler, M., et al. (2023). Modular approach to creating functionalized surface arrays of molecular qubits. Adv. Mater. **35**:2208998.

48. Poryvaev, A.S., Gjuzi, E., Polyukhov, D.M., et al. (2021). Blatter-radical-grafted mesoporous silica as prospective nanoplatform for spin manipulation at ambient conditions. Angew. Chem. Int. Ed. **60**: 8683–8688. DOI: 10.1002/anie.202015058.